Uni-directional transport properties of a serpent billiard

Uni-directional transport properties of a serpent billiard

Martin Horvat and Tomaž Prosen

Physics Department, Faculty of Mathematics and Physics, University of Ljubljana, Slovenia

E-mail: martin@fiz.uni-lj.si and prosen@fiz.uni-lj.si

Abstract
We present a dynamical analysis of a *classical billiard chain—a channel* with
parallel semi-circular walls, which can serve as a model for a bent optical fibre.
An interesting feature of this model is the fact that the phase space separates
into two disjoint invariant components corresponding to the left and right uni-
directional motions. Dynamics is decomposed into the *jump map*, a Poincaré
map between the two ends of a basic cell, and the *time function*, travelling time
across a basic cell of a point on a surface of section. The jump map has a mixed
phase space where the relative sizes of the regular and chaotic components
depend on the width of the channel. For a suitable value of this parameter, we
can have almost fully chaotic phase space. We have studied numerically the
Lyapunov exponents, time auto-correlation functions and diffusion of particles
along the chain. As a result of the singularity of the time function, we obtain
marginally normal diffusion after we subtract the average drift. The last result
is also supported by some analytical arguments.

PACS numbers: 05.45.Pq, 05.45.Gg, 05.60.Cd

1. Introduction: uni-directional billiard channels

The discussion of classical and quantum dynamics of spatially extended billiard chains, either
with periodicity or disorder, is a promising field of research with a variety of direct applications,
e.g. in nanophysics, fibre optics, electromagnetic cavities, etc. It is fair to say that studies
in spatially extended billiard systems have been underrepresented as compared to the vast
amount of work that has been dedicated to billiards on bounded domains. Nevertheless, one
has to mention several basic results in these types of systems. First, one can study the escape
rates from finite portions of an infinite billiard chain, such as the Lorentz channel [1]. Second,
one can study classical transport properties, such as diffusion and transport of heat along the
billiard chains in order to understand the dynamical (microscopic) origin of the macroscopic
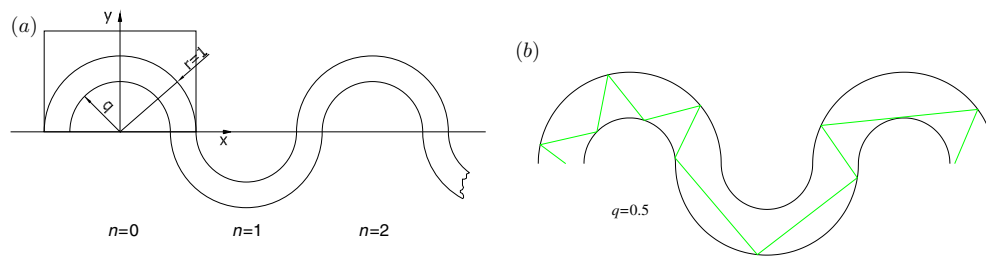
Figure 1. A schematic picture of the serpent billiard model (*a*) with one basic cell put in a rectangular frame, and index *n* labelling the consecutive cells. A typical trajectory is indicated in (*b*).

transport laws [2–4]. Third, one can study the relation between deterministic diffusion in a classical billiard chain, Anderson-like dynamical localization in the corresponding quantum chain and the nature of its spectral fluctuations [5–7]. And fourth, there is an interesting effect of localization transition in the presence of correlated disorder, which has been studied in the case of billiard chains both theoretically [8] and experimentally [9].

In this paper, we discuss a class of classical billiard channels with an unusual and distinct dynamical property, namely uni-directionality of the ray motion along the chain. Specifically, we focus our study on a particular billiard chain—a channel with parallel semi-circular walls which we name the *serpent billiard*. The billiard under discussion is built as a periodic composition of semi-circular rings of radii $q \in [0, 1)$ and 1, for the inner and outer circular arcs, respectively. The geometry of this billiard chain and an illustration of the ray dynamics are shown in figure 1. By construction, the phase space separates into two disjoint invariant components corresponding to the left and right uni-directional motions, corresponding to two different signs of the angular momentum as defined with respect to the origin (centre) of the ring of the current billiard cell. Within each cell the angular momentum is conserved. Further, it is obvious that upon the transition between one cell and another the sign of angular momentum, as calculated with respect to the centres of adjacent cells, remains unchanged. Therefore, particles travelling from left to right initially will do so forever and will thus never be able to change the direction of travel, and similarly for the motion in the opposite direction, so that these two motions constitute two disjoint invariant halves of the phase space. Nonetheless, as we shall show below, the dynamics inside each invariant half of the phase space may be (practically) totally chaotic and ergodic.

We note that this property of uni-directionality can be proved for a more general billiard channel which is bounded by an arbitrary pair of *parallel* smooth curves. Namely, it is easy to prove the following observation.

Let the billiard motion in $\mathbb{R}^2$ be bounded by two smooth C^1 curves $\mathcal{C}_j$, $j = 1, 2$, with natural parametrizations $s \to \vec{r}_j(s)$. The curves $\mathcal{C}_1$ and $\mathcal{C}_2$ should never intersect and they should be parallel in the following sense: for any $s \in \mathbb{R}$, a line $\mathcal{L}(s)$ intersecting $\mathcal{C}_1$ *perpendicularly* at $\vec{r}_1(s)$ should also intersect $\mathcal{C}_2$ *perpendicularly*, say at point $\vec{r}_2(\tau)$ defining a map $\tau = \sigma(s)$. The function $\sigma : \mathbb{R} \to \mathbb{R}$ should be a monotonically increasing invertible function, i.e. $\sigma'(s) > 0$ for all s, or in other words, the lines $\mathcal{L}(s)$ *should not intersect* each other inside the billiard region.

Then the billiard motion is *uni-directional*, i.e. the sign of the tangential velocity component $\vec{v} \cdot (\mathrm{d}/\mathrm{d}s)\vec{r}_j(s)$ stays constant for all collision points of an arbitrary trajectory.

To prove this observation, it is sufficient to consider two subsequent collisions of a segment of trajectory with a velocity of unit length $|\vec{v}| = 1$. We may assume the first collision to take
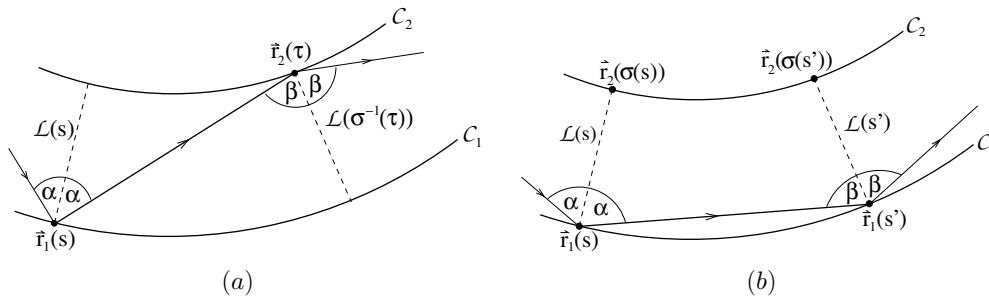
Figure 2. The schematic diagram shows two possible cases (*a*) and (*b*) of subsequent collisions needed for the proof of uni-directionality.

place at $\vec{r}_1(s) \in \mathcal{C}_1$ and write $\sin \alpha := \vec{v} \cdot (\mathrm{d}/\mathrm{d}s)\vec{r}_1(s) > 0$. Then we consider two possible cases.

(a) The next collision happens on the curve $\mathcal{C}_2$, say at the point $\vec{r}_2(\tau)$. Then the angle of incidence is again written as $\sin \beta := \vec{v} \cdot (\mathrm{d}/\mathrm{d}\tau)\vec{r}_2(\tau)$. α and β are the angles between the segment of the trajectory and lines $\mathcal{L}(s)$ and $\mathcal{L}(\sigma^{-1}(\tau))$, respectively. Since the latter two do not cross inside the billiard region, it follows that the sign of α and β should be the same (positive). We may have $\beta = 0$ only if $\alpha = 0$, i.e. when the motion takes place along $\mathcal{L}(s)$ which is a periodic orbit (see figure 2(*a*)).

(b) Another possibility is that the next collision happens with the same curve, i.e. at $\vec{r}_1(s')$. Writing $\sin \beta = \vec{v} \cdot (\mathrm{d}/\mathrm{d}s)\vec{r}_1(s')$, we again observe that the sign of the angles α and β should be the same (positive), considering that the other ends of the lines $\mathcal{L}(s)$ and $\mathcal{L}(s')$ at points $\vec{r}_2(\sigma(s))$ and $\vec{r}_2(\sigma(s'))$ should lie on the same side of the trajectory segment since the latter should not cross $\mathcal{C}_2$ (see figure 2(*b*)).

Thus, we have proved that $\mathcal{L}(s)$ is a family of marginally stable periodic orbits, of vanishing overall measure, which separates the phase space of the billiard into two halves of uni-directional motions. It is perhaps worth stressing that the conditions of parallelism as expressed in the statement also imply that the width of the channel should be constant, $|\vec{r}_1(s) - \vec{r}_2(\sigma(s))| = \text{const}$.

We should note that a detailed understanding of the dynamics of such a class of billiards may have useful applications, particularly in fibre optics, electromagnetic waveguide propagation, etc. In the following sections, we shall concentrate on the dynamics of the specific serpent billiard model, which we shall analyse in terms of a special version of the Poincaré map, the so-called jump map. Then, we shall describe analytically and numerically the average transport velocity, deterministic diffusion and correlation functions of the model.

2. Dynamics of the serpent billiards

Let us consider the Hamiltonian dynamics of a particle in a serpent billiard channel. We are considering a classical point particle with a fixed velocity of unit size. Due to the uni-directionality of the motion, as shown above, we may freely choose to consider only forward propagation—in the positive direction of the *x*-axis—as shown in the example of figure 1(*b*). The forward dynamics of the billiard can be written in terms of dynamics within a given basic cell and a transition to an adjacent basic cell. In order to fully describe the dynamics, we only need to know a Poincaré-like transformation which maps coordinates of an entry into a cell to

the coordinates of an exit and the time spent between entry and exit (the entry into an adjacent cell). Thus, we formulate the dynamics of our billiard chain in terms of a jump map model [10]. We shall define the jump map more precisely below.

Let the particle enter the basic cell on the left end at the initial position x and with the horizontal velocity component v_x and travel to the right end where it exits at the position x' and velocity v'_x. To clarify the notation, we introduce a phase space *entry section* $\mathcal{S}_L$ and an *exit section* $\mathcal{S}_R$

$$\mathcal{S}_L = \{(x, v_x) : x \in [-1, -q], v_x \in [-1, 1]\} \qquad \mathcal{S}_R = \{(x, v_x) : x \in [q, 1], v_x \in [-1, 1]\}.$$

The dynamical mapping of an entry point to an exit point shall be denoted by $\mathbf{G} : \mathcal{S}_L \to \mathcal{S}_R$,

$$(x', v'_x) = \mathbf{G}(x, v_x). \tag{1}$$

The map $\mathbf{G}$ can be expressed analytically since the billiard in the circular ring is integrable. Since the lengthy expression is not very illuminating, we give its explicit form in the appendix. In order to apply $\mathbf{G}$ again, we have to transform the current exit position x' to the entry position of the next basic cell by a map $\mathbf{S} : \mathcal{S}_R \to \mathcal{S}_L$

$$(x'', v''_x) = \mathbf{S}(x', v'_x) = (x' - 1 - q, v'_x).$$

With this transformation the conservation of angular momentum around the centre of the current cell is broken which implies non-integrability of the model. We should mention that our serpent billiard falls into the category of *semi-separable* systems [11]. The propagation of a particle from one basic cell to another can then be stated in terms of a single map $\mathbf{F} : \mathcal{S}_L \to \mathcal{S}_L$

$$\mathbf{F} = \mathbf{S} \circ \mathbf{G}. \tag{2}$$

We will refer to $\mathbf{F}$ as a *jump* or *Poincaré map* and to the phase space $\mathcal{S}_L$ as a *surface of section* (SOS). In terms of the map $\mathbf{F}$, the dynamics over the whole channel is decomposed into spatially equidistant snapshots. In order to maintain the whole physical information about the dynamics, we have to introduce the *time function* $T : \mathcal{S}_L \to \mathbb{R}^+$, i.e. $T(\mathbf{x})$ measures the time needed by a particle to travel from the entry point $\mathbf{x} = (x, v_x) \in \mathcal{S}_L$ to the other end of the basic cell. The pair $(\mathbf{F}, T)$ now represents the *jump model* corresponding to our billiard channel. Again, the time function $T(\mathbf{x})$ could be written explicitly, though with a cumbersome expression, so we put it in the appendix. However, we should note that numerical routines for computing the map $\mathbf{F}$ and the function T are very elementary and efficient.

As a useful illustration of the gross dynamical features of the model, we plot in figure 3 the phase portraits of the Poincaré-jump map $\mathbf{F}$ for different values of the parameter q. We observe that the jump map has, in general, a mixed phase space with chaotic and regular regions coexisting on SOS. We also observe that the phase portraits are symmetric in x around the mean radius $(1+q)/2$. We note that the chaotic component is always dominant in size over the regular components and for certain regions of parameter q values the regular components are practically negligible, so the jump map appears to become (almost) fully chaotic and ergodic. One nice example where we were unable to locate a single regular island has the parameter value $q = 0.6$. In figure 4 we plotted the relative area of regular SOS components as a function of the parameter q.

In order to quantify the exponential instability of trajectories inside the chaotic component of SOS, we have measured the average Lyapunov exponent λ (as described e.g. in [12]). The result for λ as a function of q is shown in figure 5. We observe that the chaoticity as measured by λ, being equal to the dynamical Kolmogorov–Sinai entropy, is always positive and is increasing monotonically with q. This trend was somehow intuitively expected, as the number of collisions within the jump increases with q. Namely, the larger number of collisions between
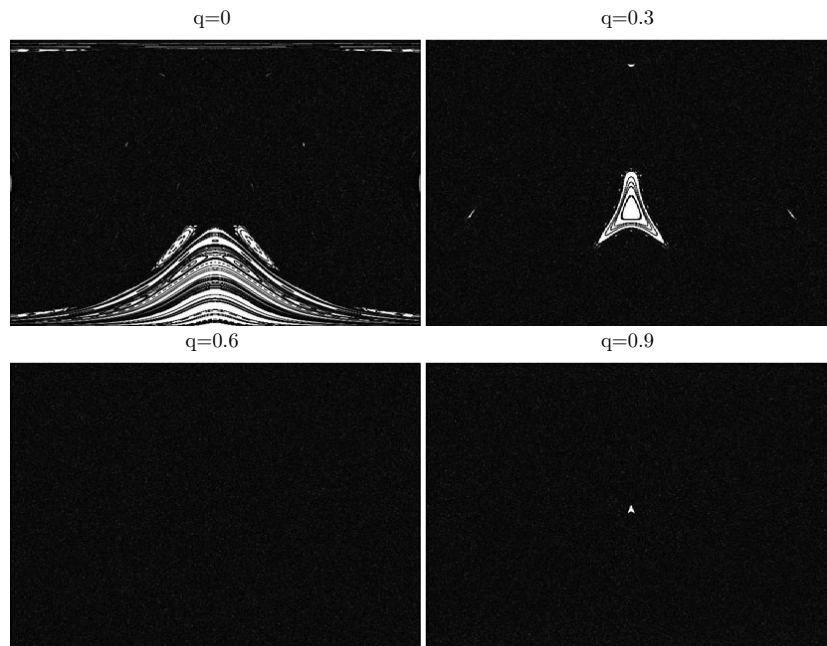
q=0   q=0.3

q=0.6   q=0.9

Figure 3. Gallery of phase space portraits of the jump map **F** for different values of the parameter q. Horizontal axis: x, vertical axis: v_x. Each diagram shows 10^4 successive iterations of 400 different initial points distributed randomly over SOS.
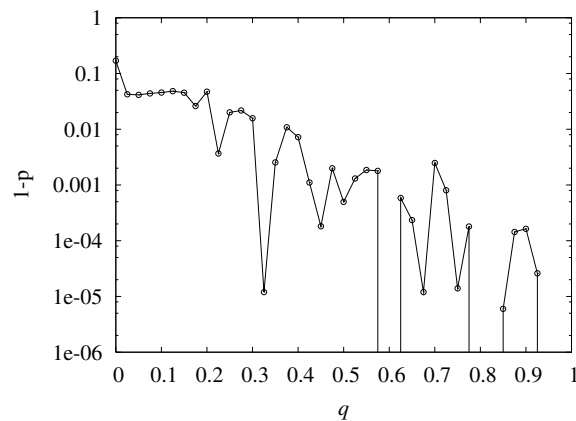

Figure 4. Numerical estimation of the total relative area of regular SOS components $1 - p$, where p is the relative area of the chaotic component of SOS, for the jump map is shown as a function of the parameter q. The ratio is obtained by sampling 1000 random trajectories starting inside the chaotic component over a phase space grid of size 1000×1000. The length of trajectories in number of jumps was 10^6.

entry and exit sections implies less correlation between the angular momenta of the adjacent cells meaning stronger integrability breaking.

Important fingerprints of dynamics, in many ways complementary to Lyapunov exponents, are the time correlation functions. These reflect the mixing property of the system which
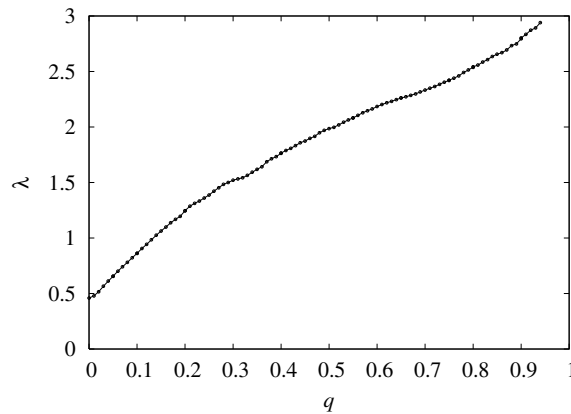
Figure 5. Lyapunov exponent λ of the jump map $\mathbf{F}$ averaged over the dominating chaotic component of SOS as a function of the parameter q. The average was computed from 1000 trajectories of length 10^5.

implies decay to equilibrium of an arbitrary initial phase space measure. The time correlation functions are also directly related to transport, which is studied in the next section, through a linear response formalism. We discuss the discrete time correlation function of the jump map between two observables $\phi(\mathbf{x})$ and $\psi(\mathbf{x})$, which is defined as

$$C_{\phi,\psi}(\tau, \mathbf{x}) = \lim_{t \to \infty} \frac{\sum_{k=0}^{t-1} \phi(\mathbf{F}^{(k)}(\mathbf{x})) \psi(\mathbf{F}^{(k+\tau)}(\mathbf{x}))}{\sum_{k=0}^{t-1} \phi(\mathbf{F}^{(k)}(\mathbf{x})) \psi(\mathbf{F}^{(k)}(\mathbf{x}))}. \tag{3}$$

The correlation functions are normalized such that always, $C_{\phi,\psi}(0, \mathbf{x}) \equiv 1$, even for observables which are not in $L^2(\mathcal{S}_L)$. In the following, we consider auto-correlation functions of very regular observables such as the phase space coordinates, namely $C_{x,x}$ and C_{v_x,v_x}, and the auto-correlation function of the time function $C_{T,T}$ which is even more interesting for two reasons: (i) $C_{T,T}$ is directly related to particle transport as described in the next section, and (ii) T is not in $L^2(\mathcal{S}_L)$ as discussed below. Numerical data presented in figure 6 strongly suggest that the correlation function $C_{T,T}$ typically exhibits exponential decay $\sim \exp(-\mathrm{const}\,\tau)$ for most of the values of q, except that for small parameter values $q < 0.3$ the initial exponential-like decay seems to turn into an asymptotic power-law decay $\sim t^{-\mathrm{const}}$. On the other hand the correlation decay of non-singular observables, such as $C_{x,x}$ and C_{v_x,v_x}, seems to behave as a power law for all values of q. It is interesting to observe that the qualitative nature of correlation decay seems to be quite different for different classes of observables such as x compared to T. However, in all cases time correlation functions strongly decay which is a firm indication of the mixing property of the serpent billiard on the chaotic component.

The time function $T(\mathbf{x})$ is expected to have a singularity for $v_x \to \pm 1$ as it may take arbitrarily long to traverse the semi-circular ring with a sufficiently small value of angular momentum. It is straightforward to show that this is a square-root singularity

$$T(x, v_x) \sim (1 - |v_x|)^{-1/2} \qquad |v_x| \sim 1. \tag{4}$$

An example of the structure of the time function for $q = 0.6$ is shown as a density plot in figure 7(a). Another quantity which can illustrate the dynamical behaviour of observable T is the probability distribution $P(T)$ of times $T(\mathbf{x})$ for a very long chaotic trajectory. Assuming that the system is ergodic on the full SOS, the probability distribution $P(T)$ can be written in
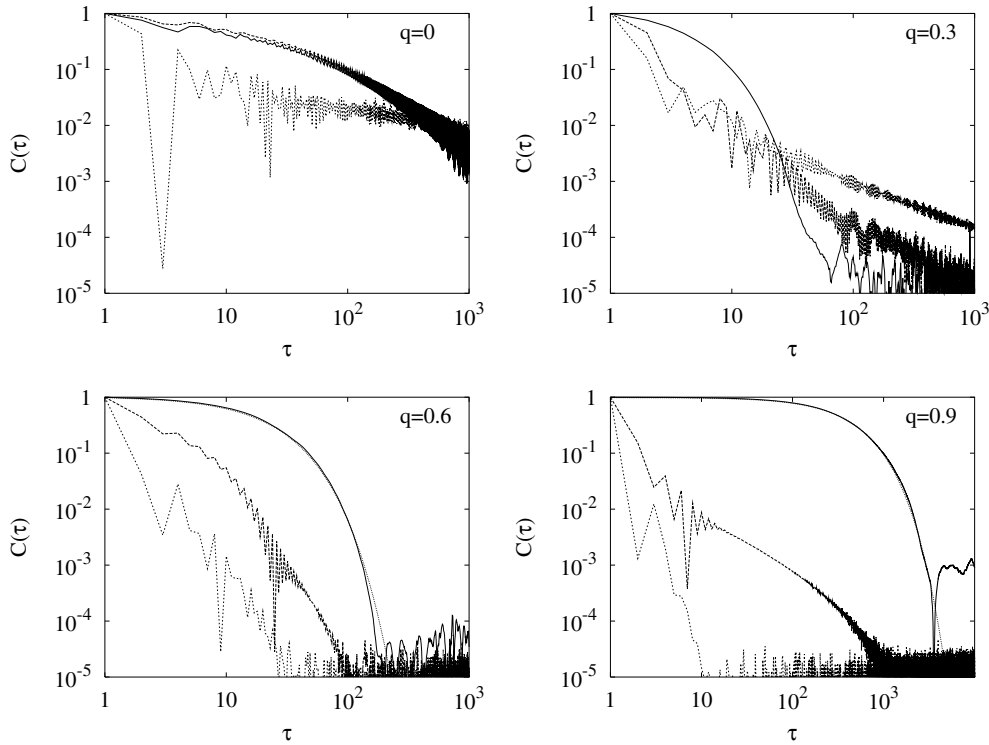
Figure 6. The average auto-correlation functions: $\langle C_{T,T}(\mathbf{x}, \tau)\rangle_\Omega$ (full curve), $\langle C_{x,x}(\mathbf{x}, \tau)\rangle_\Omega$ (dashed) and $\langle C_{v_x, v_x}(\mathbf{x}, \tau)\rangle_\Omega$ (dots) as functions of the number of jumps τ. The calculation is performed using trajectories of length 5×10^5 and averaged over 10^4 initial conditions $\mathbf{x}$ over the chaotic SOS component. In the plot for $q = 0.6$ and $q = 0.9$ we insert the exponentials $\exp(-0.050\,8193\tau)$ and $\exp(-0.002\,341\,54\tau)$, respectively, in order to guide the eye. The noisy plateaus indicate the level of statistical fluctuation.

terms of the constant invariant measure on SOS

$$P(t) = \int \delta(t - T(\mathbf{x}))\, \mathrm{d}^2\mathbf{x}. \tag{5}$$

Singularity (4) implies the asymptotic form of the distribution

$$P(t) \sim t^{-3} \tag{6}$$

for large t. This asymptotic property does not essentially depend on the full ergodicity of the map, as we find the same asymptotic behaviour by numerical simulation of $P(t)$ for different values of q as shown in figure 7(b). It is obvious that the only important condition for the universal decay of $P(t)$ is that the chaotic component should extend to the lines of singularity $v_x = \pm 1$. The distribution $P(t)$ is very important, because it directly connects to the particle transport properties of the channel that are discussed in the next section.

3. Transport properties

Here we would like to examine the transport properties along our billiard chain in the context of the jump model. The basic cells are labelled with a non-negative integer $n \in \mathbb{Z}^+$ starting with $n = 0$ and counting forward to the right. The transported length is measured as the
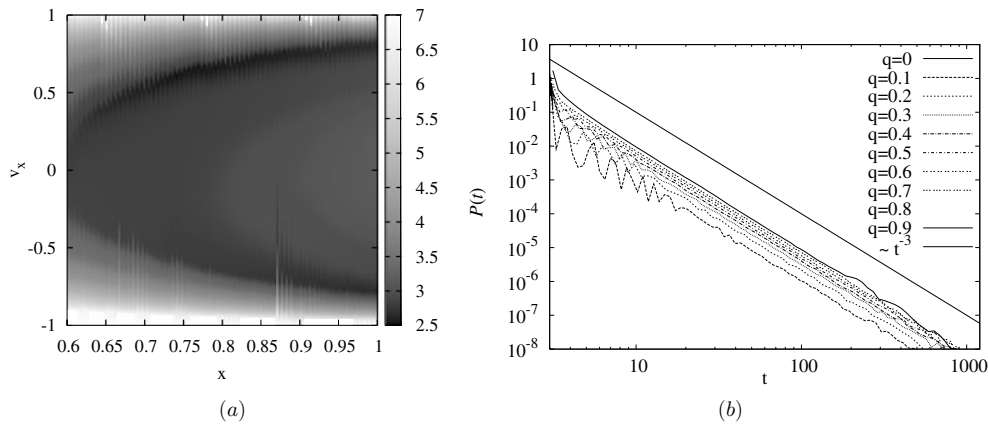
Figure 7. (a) Density plot of the time function on a logarithmic scale at $q = 0.6$ and (b) the distribution $P(t)$ of the values of the time function for different q indicated in the figure. The thicker full straight line indicates t^{-3} decay.

number of traversed basic cells. This means that our length of travel is an integer but we should keep in mind that the physical length of one basic cell in the direction along the chain is $1 + q$.

Let us prepare an ensemble of particles on the SOS $\mathcal{S}_L$ of the zeroth basic cell, $n = 0$. The phase space is generally mixed and let the dominating chaotic component be denoted by $\Omega \subset \mathcal{S}_L$. We observe that each invariant phase space component may have its own transport properties and to obtain a clear picture of transport we have to test each component separately. The transport on regular components (islands) of SOS is obviously ballistic since the islands are transporting with a constant and sharply defined average velocity. Thus we concentrate on the more nontrivial case of transport on the chaotic component, namely in the following, we choose a uniform initial distribution of the particles over the leading chaotic component Ω: $\mu(\mathrm{d}^2\mathbf{x}) = \mathrm{d}^2\mathbf{x}/\mathrm{vol}(\Omega)$.

The transport of an ensemble of particles is described using the probability distribution $P(n, t)$ of particles over the basic cells $n \in \mathbb{Z}^+$ as a function of time t. Let us express this distribution in terms of a jump map $\mathbf{F}(\mathbf{x})$ and the time function $T(\mathbf{x})$. The time spent by a particle to traverse m basic cells starting from the initial position $\mathbf{x} \in \mathcal{S}_L$ is calculated as

$$T_m(\mathbf{x}) = \sum_{k=0}^{m-1} T(\mathbf{F}^{(k)}(\mathbf{x})). \tag{7}$$

The probability distribution of a single particle with initial coordinate $\mathbf{x}$ over the basic cells (labelled by $n \in \mathbb{Z}^+$) at time t can be written straightforwardly as

$$P(n, t, \mathbf{x}) = \int_0^t \{\delta(\tau - T_n(\mathbf{x})) - \delta(\tau - T_{n+1}(\mathbf{x}))\} \, \mathrm{d}\tau. \tag{8}$$

By averaging $P(n, t, \mathbf{x})$ over an initial ensemble of particles, defined by

$$\langle f(\mathbf{x}) \rangle_\Omega := \int_\Omega \mu(\mathrm{d}^2\mathbf{x}) f(\mathbf{x}) \tag{9}$$

we obtain the distribution of particles over the cells

$$P(n, t) = \langle P(n, t, \mathbf{x}) \rangle_\Omega = \int_0^t \{p_n(\tau) - p_{n+1}(\tau)\} \, \mathrm{d}\tau \tag{10}$$

where we are using the ensemble average distribution of times needed to traverse n basic cells, denoted as $p_n(t)$,

$$p_n(t) = \langle \delta(\tau - T_n(\mathbf{x})) \rangle_\Omega. \tag{11}$$

Let $\langle \bullet \rangle_P$ denote an average over the spatial distribution $P(n, t)$

$$\langle f(n) \rangle_P = \sum_{n=0}^{\infty} f(n) P(n, t). \tag{12}$$

Our aim is to obtain the time-asymptotic ($t \to \infty$) form of $P(n, t)$ where only contributions of far lying cells $n \gg 1$ are relevant. Since the auto-correlation functions in our model are decaying very fast, in particular the relevant $\langle C_{T,T}(\mathbf{x}, t) \rangle_\Omega$ (see the end of the previous section), we may employ the central limit theorem and approximate the distribution of T_n, $p_n(t)$, in terms of the distribution of T, $p_1(t) = \langle \delta(t - T(\mathbf{x})) \rangle_\Omega$.

$$p_n(t) = \underbrace{(p_1 * \cdots * p_1)}_{n}(t) \qquad n \gg 1. \tag{13}$$

This approximation is very useful, because we can obtain the whole distribution $P(n, t)$ using a single function $p_1(t) = P(t)$ that can be easily measured and is already plotted in figure 7(b). In the limit $n \to \infty$, we can treat the variable T_n as infinitely divisible [13] and the parameter n as a continuous variable. Then we can approximate the finite difference in n in equation (10) in terms of a derivative ∂/∂_n and calculate $P(n, t)$ as

$$P(n, t) \approx -\frac{\partial}{\partial n} \int_0^t p_n(\tau) \, d\tau. \tag{14}$$

The basic properties of the transport shall be described by the mean traversed length $\langle n \rangle_P$ and the spatial spread of the initial ensemble $\sigma_n^2 = \langle n^2 \rangle_P - \langle n \rangle_P^2$. The mean $\langle n \rangle_P$ can be asymptotically, for $t \to \infty$, exactly expressed by the formula

$$\langle n \rangle_P = \int_0^t \sum_{n=0}^{\infty} p_n(\tau) \, d\tau. \tag{15}$$

From the central limit theorem, we immediately obtain the mean velocity as the inverse mean traverse time

$$v = \lim_{t \to \infty} \frac{\langle n \rangle_P}{t} \qquad t_{\text{mean}} = \frac{1}{v} = \int_0^{\infty} t p_1(t) \, dt \tag{16}$$

The average t_{mean}, and the minimal time t_{min} to traverse a basic cell, as a function of q are plotted in figure 8. The mean time t_{mean} is almost linearly increasing with increasing parameter q. This reflects the obvious fact that the travel becomes slower by narrowing the channel. The fact that the linear growth of $\langle n \rangle_P$ is indeed given by velocity v is also demonstrated numerically for $q = 0.6$ in figure 9(a). It is a little more tedious to obtain an analytical approximation for the average spreading width $\sigma_n^2(t) = \langle n^2 \rangle_P - \langle n \rangle_P^2$.

Essentially, we need to control the growth of the second moment of distribution $P(n, t)$. This distribution is given by equation (14) in terms of $p_n(t)$ which may be asymptotically expressed as a convolution of independent distributions $p_1(t)$ (13) assuming sufficiently fast decay of temporal correlations as established numerically. As a consequence, $p_n(t)$ inherits cubic singularity of $p_1(t)$, namely $p_n(t) \propto t^{-3}$. This heuristic argument would suggest marginally normal diffusion $\sigma_n^2(t) \propto t \log t$, not essentially connected to the strength of correlation decay but simply as a consequence of singularity of the time function.

This observation can be formalized with a brief calculation. We stress that for large times $t \to \infty$, only cells with labels $n \sim vt \gg 1$ contribute appreciably to the probability
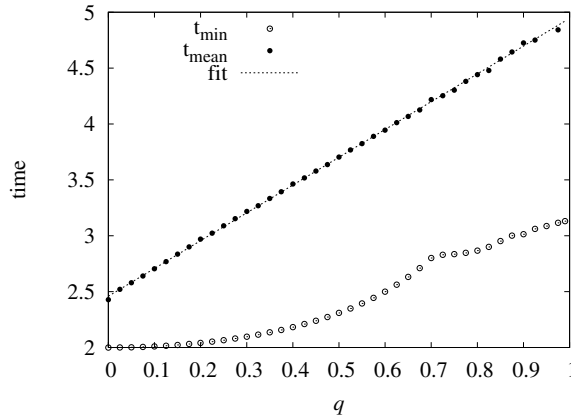
Figure 8. Minimal time t_{min} and average time t_{mean} for traversing a basic cell over the chaotic SOS component are shown as functions of the parameter q. The curve that fits t_{mean} is the linear function $2.458\,63 + 2.486\,96q$. The averaging and minimizing are performed on a trajectory of length 10^7.
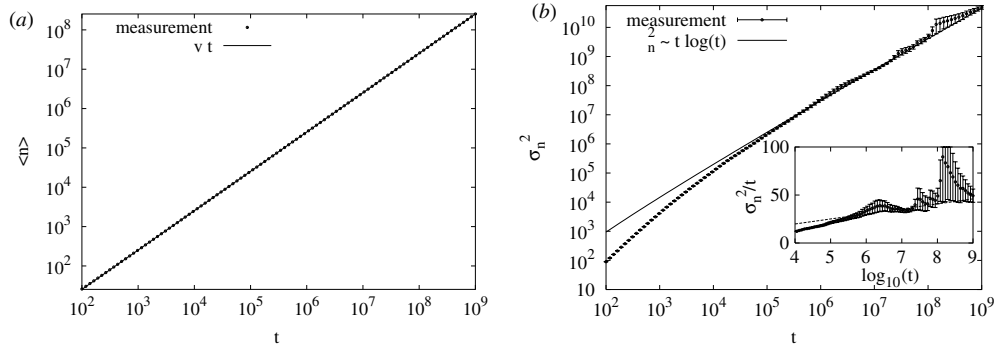

Figure 9. The average position $\langle n \rangle_P$ (a) and the spread of particles $\sigma_n^2 = \langle n^2 \rangle_P - \langle n \rangle_P^2$ (b) as a function of time t at $q = 0.6$. The average transport velocity $v = 1/t_{mean}$, where $t_{mean} = 3.945\,38$ is obtained from the data of figure 8. The error bars represent the standard deviation of the measurement. The statistics is performed over an ensemble of 25 000 initial points. The fitted line in the inset is given by $\sigma_n^2/t = -0.044\,374 + 5.2636 \log_{10} t$.

distribution $P(n, t)$. In this regime we approximate $p_n(t)$ using (13), hence we can easily write its Fourier transform as

$$\hat{p}_n(k) = (\hat{p}_1(k))^n = \exp(n \log \hat{p}_1(k)) \qquad \hat{f}(k) = \int_{-\infty}^{\infty} \exp(ikt) f(t) \, dt. \tag{17}$$

The asymptotics of $\hat{p}_1(k)$ for $k \to 0$ will determine the asymptotics for $p_n(t)$ for long times $t \to \infty$. Thus we write the local expansion of $\hat{p}_1(k)$ around $k = 0$ explicitly taking into account the known asymptotics in the time domain, $p_1(t \to \infty) \sim t^{-3}$, namely

$$\log \hat{p}_1(k) = it_{mean}k + \sigma_0^2 k^2(\alpha + \log k) + O(k^3) \qquad k > 0 \tag{18}$$

where σ_0^2 and α are positive constants depending on the details of $p_1(t)$. Using equations (18) and (17) and applying the inverseOurier transform we find that the limiting distribution, namely p_n for large n, is given by the formula

$$p_n(t) = \frac{1}{\sigma_t} g\left(\frac{t - nt_{mean}}{\sigma_t}\right) \qquad \sigma_t^2 = \sigma_0^2 n \log n \qquad \text{for} \quad n \gg 1. \tag{19}$$

where $g(x) = \frac{1}{\sqrt{2\pi}} \exp(-x^2/2)$ is the standard Gaussian function. By inserting the above expression (19) into the approximation of $P(n, t)$ (14) and expanding in terms of parameter $n - vt$ we get the result

$$P(n, t) = \frac{1}{\sigma_n} g\left(\frac{n - vt}{\sigma_n}\right) \qquad \sigma_n^2 = \sigma_0^2 v^3 t \log(vt) \qquad \text{for} \quad n \gg 1. \quad (20)$$

From this analysis we predict that the diffusion of initial ensemble of particles will distribute over the basic cells with dispersion growing as $t \log t$. Thus we have shown analytically that our serpent billiard exhibits marginally normal diffusion with a drift.

We have tested our analytical results by performing extensive numerical simulations. An example of $\sigma_n^2(t)$ for $q = 0.6$ is shown in figure 9(b). We stress that our numerical data are indeed consistent with the marginally normal diffusion.

4. Summary and discussion

In this paper we have analysed a simple billiard chain, the so-called serpent billiard, with a special dynamical property of strictly uni-directional classical motion. We have also proved the uni-directionality of motion for a more general class of billiard channels with parallel walls. The dynamics along the serpent billiard channel is described in terms of a variant of a jump model [10], namely, the jump-Poincaré map between the surfaces of section of two adjacent basic cells of the billiard, and the time function, i.e. the time needed to traverse the basic cell as a function of the position on the surface of section. We have shown that the jump map is chaotic with generally mixed phase space, where the relative size of the largest chaotic component is generally increasing with decreasing channel width. The latter dependence is not strictly monotonic, because of bifurcations of regular components, but for narrow channels the chaotic component is typically largely dominant. For a considerable range of the parameter (denoting the channel width) the jump map is even practically fully chaotic, ergodic, as no detectable islands of regular motion have been found. This does not mean that the islands of stability cannot exist for typical values of the parameter. We only wish to stress that it is easy to find parameter values (such as the case $q = 0.6$ studied in the paper) for which all possible islands of stability are undetectably small for numerical (experimental) purposes. Numerically measured maximal Lyapunov exponent shows that the chaoticity on a chaotic component is monotonically increasing with narrowing channel.

The transport of particles along the channel measured in the number of traversed basic cells exhibits a marginally normal diffusion $\sigma_n^2 \sim t \log t$ (when the drift term is subtracted) due to the square-root singularity of the time function. This singularity is a consequence of parallel walls, or putting it in dynamical terms, it is due to a family of marginally stable bouncing ball trajectories bouncing perpendicularly between the walls.

Besides its interesting and rather exotic dynamical properties, the model and its generalizations may also be relevant for real world problems of transport, such as in optical fibres or waveguides. These results may open even more interesting questions on the properties of quantum or wave transport of classically uni-directional billiard channels. This is the subject of a subsequent publication [14].

Acknowledgments

Appendix. Explicit jump map and time function

Let the particle enter the basic cell at point $\mathbf{x} = (x, \cos\phi) \in \mathcal{S}_L$ and exit at point $\mathbf{x}' = (x', \cos\phi') \in \mathcal{S}_R$. Here we explicitly write the map $\mathbf{G}: \mathbf{x} \to \mathbf{x}'$, equation (1), and the time function $T(\mathbf{x})$. Due to conservation of the angular momentum within a fixed cell, we have the relation

$$\Gamma = -x \sin\phi = x' \sin\phi'$$

so we just have to give an explicit formula for the map $g: \phi \to \phi'$ and the time function $t(\phi)$. Then the remaining relation to specify the full map G simply reads $x' = -x \sin\phi / \sin g(\phi)$. Let us write some auxiliary variables

$$\beta = \arcsin\Gamma \qquad \gamma = \arcsin(\Gamma/q)$$
$$\alpha' = \alpha + n\delta \qquad n = \left\lfloor \frac{\pi - \alpha}{\delta} \right\rfloor$$

where $\lfloor x \rfloor$ is the largest integer not larger than x, and α and δ are determined for each case separately below.

If $\Gamma > q$, the particle is only hitting the outside wall. Then, writing $\alpha = \pi - \phi - \beta$, $\delta = \pi - 2\beta$, we have

$$\phi' = (n+1)\delta - \phi$$
$$t = \sqrt{1 + x^2 + 2x\cos\alpha} + \sqrt{1 + x'^2 + 2x'\cos\alpha'} + 2n\cos\beta.$$

In the opposite case where $\Gamma < q$, writing $\delta = \gamma - \beta$ and $\Delta t = \sqrt{1 + q^2 - 2q\cos\delta}$, we have to discuss two cases: (i) when the particle first hits the inner wall, $\phi < \pi/2$

$$\phi' = \begin{cases} (n+1)\delta - \phi & n \text{ odd} \\ 2\gamma - \pi + n\delta - \phi & n \text{ even} \end{cases}$$
$$t = \sqrt{q^2 + x^2 + 2xq\cos\alpha} + n\Delta t + \begin{cases} \sqrt{1 + x'^2 + 2x'\cos\alpha'} & n \text{ odd} \\ \sqrt{q^2 + x'^2 + 2x'q\cos\alpha'} & n \text{ even} \end{cases}$$

and (ii) when the particle first hits the outer wall, $\phi \geqslant \pi/2$

$$\phi' = \begin{cases} (n+1)\delta - \phi & n \text{ odd} \\ \pi - 2\beta + n\delta - \phi & n \text{ even} \end{cases}$$
$$t = \sqrt{1 + x^2 + 2x\cos\alpha} + n\Delta t + \begin{cases} \sqrt{q^2 + x'^2 + 2x'q\cos\alpha'} & n \text{ odd} \\ \sqrt{1 + x'^2 + 2x'\cos\alpha'} & n \text{ even}. \end{cases}$$

where α is equal to $\gamma - \phi$ in case (i) and $\pi - \phi - \beta$ in case (ii).

References

[1] Gaspard J P 1993 What is the role of chaotic scattering in irreversible processes? *Chaos* **3** 427–42
[2] Alonso D, Artuso R, Casati G and Guarneri I 1999 Heat conductivity and dynamical instability *Phys. Rev. Lett.* **82** 1859–62
[3] Alonso D, Ruiz A and de Vega I 2002 Polygonal billiards and transport: diffusion and heat conduction *Phys. Rev.* E **66** 066131
[4] Li B, Casati G and Wang J 2003 Heat conductivity in linear mixing systems *Phys. Rev.* E **67** 021204
[5] Dittrich T, Doron E and Smilansky U 1994 Classical diffusion, Anderson localization, and spectral statistics in billiard chains *J. Phys. A: Math. Gen.* **27** 79–114

[6] Dittrich T, Mehlig B, Schanz H and Smilansky U 1997 Universal spectral properties of spatially periodic quantum systems with chaotic classical dynamics *Chaos Solitons Fractals* **8** 1205–27

[7] Dittrich T, Mehlig B, Schanz H and Smilansky U 1998 Signature of chaotic diffusion in band spectra *Phys. Rev. E* **57** 359–65

[8] Izrailev F M 2003 Onset of delocalization in quasi-one-dimensional waveguides with correlated surface disorder *Phys. Rev. B* **67** 113402

[9] Kuhl U, Izrailev F M, Krokhin A A and Stöckmann H-J 2000 Experimental observation of the mobility edge in a waveguide with correlated disorder *Appl. Phys. Lett.* **77** 633–5

[10] Zumofen G and Klafter J 1993 Scale-invariant motion in the intermittent chaotic systems *Phys. Rev. E* **47** 851–63

[11] Prosen T 1996 Quantum surface of section method: Eigenstates and unitary quantum Poincaré evolution *Physica D* **91** 244–77

[12] Reichl L E 1992 The transition to chaos *Conservative Classical Systems: Quantum Manifestations* (New York: Springer)

[13] Feller W 1966 *An Introduction to Probability Theory and its Applications* (New York: Wiley)

[14] Horvat M and Prosen T in preparation